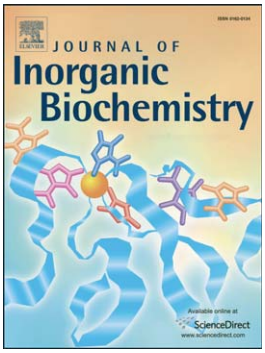

New 4′-(4-chlorophenyl)-2,2′:6′,2″-terpyridine ruthenium(II) complexes: Synthesis, characterization, interaction with DNA/BSA and cytotoxicity studies

Milan M. Milutinović, Ana Rilak, Ioannis Bratsos, Olivera Klisurić, Milan Vraneš, Nevenka Gligorijević, Siniša Radulović, Živadin D. Bugarčić

PII: S0162-0134(16)30330-0
DOI: doi:10.1016/j.jinorgbio.2016.10.001
Reference: JIB 10091

To appear in: *Journal of Inorganic Biochemistry*

Received date: 8 June 2016
Revised date: 6 October 2016
Accepted date: 13 October 2016

Please cite this article as: Milan M. Milutinović, Ana Rilak, Ioannis Bratsos, Olivera Klisurić, Milan Vraneš, Nevenka Gligorijević, Siniša Radulović, Živadin D. Bugarčić, New 4′-(4-chlorophenyl)-2,2′:6′,2″-terpyridine ruthenium(II) complexes: Synthesis, characterization, interaction with DNA/BSA and cytotoxicity studies, *Journal of Inorganic Biochemistry* (2016), doi:10.1016/j.jinorgbio.2016.10.001

New 4'-(4-chlorophenyl)-2,2':6',2''-terpyridine ruthenium(II) complexes: Synthesis, characterization, interaction with DNA/BSA and cytotoxicity studies

Milan M. Milutinović [a], Ana Rilak [a,*], Ioannis Bratsos [b], Olivera Klisurić [c], Milan Vraneš [d], Nevenka Gligorijević [e], Siniša Radulović [e], Živadin D. Bugarčić [a,*]

[a] *Faculty of Science, University of Kragujevac, R. Domanovića 12, P. O. Box 60, 34000 Kragujevac, Serbia.*

[b] *I.N.N., Dept. of Physical Chemistry, NCSR "Demokritos", 15310 Ag. Paraskevi, Athens, Greece.*

[c] *Department of Physics, Faculty of Sciences, University of Novi Sad, Trg Dositeja Obradovića 4, 21000 Novi Sad, Serbia.*

[d] *University of Novi Sad, Faculty of Sciences, Department of Chemistry, Biochemistry and Environmental Protection, Trg Dositeja Obradovića 3, 21000 Novi Sad, Serbia.*

[e] *Institute for Oncology and Radiology of Serbia, Pasterova 14, 11000 Belgrade, Serbia.*

* Corresponding authors:

Prof. Dr. Živadin D. Bugarčić, E-mail: bugarcic@kg.ac.rs
Fax: +381(0)34335040; Tel: +381(0)34300262

Dr. Ana Rilak, E-mail: anarilak@kg.ac.rs ; Fax: +381(0)34335040; Tel: +381(0)34300262

Abstract

In this study, we have developed a series of new monofunctional Ru(II) complexes of the general formula *mer*-[Ru(Cl-Ph-tpy)(*N*-*N*)Cl]Cl in which Cl-Ph-tpy is 4'-(4-chlorophenyl)-2,2':6',2"-terpyridine, *N*-*N* is a bidentate chelating ligand (1,2-diaminoethane (en, **1**), 1,2-diaminocyclohexane (dach, **2**) or 2,2'-bipyridine (bpy, **3**)). All complexes were fully characterized by elemental analysis and spectroscopic techniques (IR, UV-Vis, 1D and 2D NMR). Their chemical behavior in aqueous solution was studied by UV-Vis and NMR spectroscopy showing that all compounds are relatively labile leading to the formation of the corresponding aqua species **1aq – 3aq**. Their DNA binding ability was evaluated by UV-Vis spectroscopy, fluorescence quenching measurements and viscosity measurements. Competitive studies with ethidium bromide (EB) showed that the complexes can displace DNA-bound EB, suggesting strong competition with EB (K_{sv} = 3.7 – 9.6 × 10^4 M^{-1}). These experiments show that the ruthenium complexes interact with DNA *via* intercalation. The complexes bind to serum protein albumin displaying relatively high binding constants (K_{sv} = 10^4 – 10^5 M^{-1}). Compound **3** displayed from high to moderate cytotoxicity against two cancer cell lines HeLa and A549 (with IC_{50} *ca*. 12.7 μM and 53.8 μM, respectively), while complexes **1** and **2** showed only moderate cytotoxicity (with IC_{50} *ca*. 84.8 μM and 96.3 μM, respectively) against HeLa cells. The cell cycle analysis (by flow cytometry) of HeLa and A549 cells treated with complex **3** shows minor changes on the cell cycle phase distribution.

Keywords: Ru(II) complexes, meridional, substituted terpyridine, DNA, Albumin, Cytotoxicity

1. Introduction

In the past two decades ruthenium coordination compounds have attracted considerable interest as potential anticancer agents because of their low toxicity and their efficacy against platinum drug-resistant tumors, reflected in promising results in various stages of preclinical to early clinical studies [1-5].

Recently, we developed a series of new polypyridyl complexes of the general formula *mer*-[Ru(L_3)(*N*-*N*)(X)][Y]*n* where L_3 is either tpy (2,2':6',2''-terpyridine) or Cl-tpy (4'-chloro-2,2':6',2''-terpyridine), *N*-*N* is a bidentate chelating ligand (1,2-diaminoethane (en), 1,2-diaminocyclohexane (dach), 2,2'-bipyridine (bpy)), X is a monodentate ligand (Cl or dmso-*S*), Y is the counter anion (Cl, PF_6 or CF_3SO_3), and *n* depends on the nature of chel and X [6,7]. It was evidenced that ruthenium complexes strongly bind DNA by a dual function: by intercalation, interacting with the DNA helix through the insertion of the planar terpyridine ring between the DNA base pairs, and by covalent binding to guanine *N*7 [7]. In addition, it was proved that these complexes can covalently bind to bovine serum albumin (BSA) through the imidazole ring of histidine [8]. The cytotoxicity of these Ru(II)-tpy complexes was studied by MTT assay using human lung carcinoma (A549), human colon carcinoma (HCT116) and mouse colon carcinoma (CT26) cell lines. It was found that only [Ru(Cl-tpy)(en)Cl]Cl and [Ru(Cl-tpy)(dach)Cl]Cl showed from high to moderate *in vitro* cytotoxicity, with IC_{50}'s of 32.80 ─ 66.30 μM and 72.80 ─ 110.80 μM, respectively [7]. It is worth noting that both Ru(II)-tpy complexes hydrolyze the chloride ligand at a reasonable rate (i.e. within minutes) and they are capable to act as hydrogen bond donors through the chelating ligand. These two features seem to be a prerequisite for antiproliferative activity [7,8].

Varying substitutive group or substituent position in the intercalative ligand can create some interesting differences in the space configuration and the electron density distribution of

Ru(II) polypyridyl complexes, which results in some differences in the behavior of the complexes in the interactions with DNA and proteins, and will be helpful to more clearly understand the binding mechanism of Ru(II) polypyridyl complexes to DNA and BSA [9-11]. The presence of electron donating substituents on the tpy fragment decreases the reactivity of the metal centre, whereas the addition of an electron withdrawing entity has the opposite effect [12-15]. Furthermore, additional functional groups, like halogens, on the tpy fragment might enhance the binding ability of the complexes on the biomolecules [6].

In this work, with the aim of further extending the structure-activity relationship of polypyridyl ruthenium compounds we have used a 4'- chlorophenyl-substituted tpy ligand, i.e. 4'-(4-chlorophenyl)-2,2':6',2''-terpyridine (Cl-Ph-tpy), to prepare three new complexes of the general formula [Ru(Cl-Ph-tpy)(*N*-*N*)Cl]Cl (where *N*-*N* = en (**1**), dach (**2**) or bpy (**3**); Fig. 1). All new complexes were fully characterized by elemental analysis and various spectroscopies, such as IR, UV-Vis, 1D and 2D NMR. Considering the importance of the hydrolysis in the mechanism of action of anticancer metal compounds, we investigated the kinetics of aquation of selected phenyl-substituted Ru(II)-tpy complexes by UV-Vis spectrophotometry, as well as the chemical behavior of all complexes in aqueous solution by ^{1}H NMR spectroscopy. The interaction of complexes **1 − 3** with calf thymus DNA (CT DNA) was studied, and a competitive study of the intercalative agent ethidium bromide (EB) was performed. Furthermore, the affinity of **1 − 3** toward bovine serum albumin was investigated, and their binding constants were determined. We report also the results of *in vitro* cytotoxicity tests performed on complexes **1 – 3** against two human cancer cell lines (human cervix carcinoma cell line (HeLa) and human lung carcinoma cells (A549)), and one normal cell line (human fetal lung fibroblast cells (MRC-5)) in comparison with their Cl-tpy analogues [Ru(Cl-tpy)(en)Cl]Cl (**4**), [Ru(Cl-tpy)(dach)Cl]Cl (**5**) and [Ru(Cl-tpy)(bpy)Cl]Cl (**6**), the respective precursor [Ru(Cl-Ph-tpy)Cl_3] (**P1**), and cisplatin. The lipophilic properties

and cytotoxic effects of the complexes are assayed in order to elucidate the relationship between structure and activity.

Fig. 1.

2. Materials and methods

1,2-diaminoethane (en), (±)-trans-1,2-diamminocyclohexane (dach), 2,2'-bipyridine (bpy), 4'-chloro-2,2':6',2''-terpyridine (Cl-tpy), 4'-(4-chlorophenyl)-2,2':6',2''-terpyridine (Cl-Ph-tpy) and bovine serum albumin (BSA) are commercially available and were used as received. The complexes [Ru(Cl-tpy)(en)Cl]Cl (**4**), [Ru(Cl-tpy)(dach)Cl]Cl (**5**) and [Ru(Cl-tpy)(bpy)Cl]Cl (**6**) were synthesized as reported previously [6]. Microanalysis, UV-Vis spectra and ^{1}H NMR spectra were used to check the purity of these complexes and the spectra agreed well with the data already reported [6]. All other chemicals were used as purchased without further purification. Doubly distilled water was used as the solvent throughout the experiments. The stock solution of CT-DNA was prepared in 5 mM Tris-HCl/50 mM NaCl buffer at pH = 7.4, which gave a ratio of UV absorbances at 260 nm and 280 nm (A_{260}/A_{280}) of *ca*. 1.8 - 1.9, indicating that the DNA was sufficiently free of protein and the concentration was determined by UV absorbance at 260 nm (ε = 6600 M^{-1} cm^{-1}) [16]. The stock solution of BSA was prepared by dissolving the solid BSA in 5 mM Tris-HCl/50 mM NaCl buffer at pH = 7.4, and the concentration was kept fixed at 2 μM. All stock solutions were stored at 4 ºC and used within 5 days.

Mono- (^{1}H; 500 MHz) and bi-dimensional (^{1}H-^{1}H COSY) NMR spectra were recorded on a Bruker Avance 500 MHz spectrometer. ^{1}H chemical shifts in D_2O were referenced to the internal standard 2,2-dimethyl-2,2-silapentane-5-sulfonate (DSS) at δ = 0.00 or to external 1,4-dioxane (δ = 3.75), whereas in CD_3CN were referenced to the peak of

residual non-deuterated solvent (δ = 1.94). All NMR spectra were run at 298 K. The UV-Vis spectra were obtained on a Perkin-Elmer Lambda 35 double beam spectrophotometer, using 1.0 cm path-length quartz cuvettes (3.0 mL). Infrared spectra were recorded on a Perkin-Elmer 983G spectrometer. Fluorescence measurements were carried out on a RF-1501 PC spectrofluorometer (Shimadzu, Japan). The excitation and emission bandwidths were both 10 nm.

2.1. Synthesis

The aqua species that are obtained in aqueous solution from some complexes upon hydrolysis of Cl^- are labelled with the same number of the parent compound followed by "aq". The NMR assignments of these species are reported in the Supporting Information (Table S1).

*2.1.1. Synthesis of [Ru(Cl-Ph-tpy)Cl_3] (**P1**)*

A 262 mg amount of $RuCl_3 \cdot 3H_2O$ (1 mmol) was dissolved in 130.0 mL of ethanol and the solution was refluxed until the color of the solution changed from brown to green (*ca*. 2 h). Then a 344.5 mg amount of Cl-Ph-tpy (1 mmol) was added and reflux continued for 5 h. During this time the color of the solution turned again to brown reddish with the simultaneous formation of the product as a brown solid. The precipitation of the product was accomplished by cooling the solution to room temperature. The solid was collected by filtration, washed with ethanol and diethyl ether and dried under vacuum. Yield: 450.6 mg (82%). Anal Calcd for $C_{21}H_{14}Cl_4N_3Ru$ (551.24) requires: C, 45.76; H, 2.56; N, 7.62. Found: C, 45.76; H, 2.59; N, 7.65. Complex [Ru(Cl-Ph-tpy)Cl_3] is soluble in DMSO and acetonitrile, slightly soluble in water, methanol, ethanol, acetone, chloroform and dichloromethane. Selected IR (KBr, cm^{-1}): ν_{tpy} 3075 (m), 2924 (w), 1600 (vs), 1467 (vs), 1426 (s), 1243 (s),

1090 (s), 789 (vs), 654 (w). UV/visible spectrum (DMSO; λ_{max}, nm (ε, M^{-1} cm^{-1})): 283 (29196), 310 (22920), 414 (6820). The product was used without further purification.

*2.1.2. General synthetic procedure for [Ru(Cl-Ph-tpy)(N-N)Cl]Cl (**1 – 3**)*

A weighed amount of [Ru(Cl-Ph-tpy)Cl_3] (**P1**) was suspended in an ethanol/H_2O (3:1) mixture containing 10 eq. of LiCl and 3 eq. of triethylamine (Et_3N). The chelating ligand *N-N* (1.2 eq.; *N-N* = en, dach, bpy) was then added and the mixture was refluxed under argon for *ca.* 5 h with vigorous stirring. The violet to purple solution was filtered while hot to remove any undissolved material. Rotary concentration under reduced pressure to *ca*. ¼ of the initial volume and storage at 4.0 °C for 24 h induced the formation of the product as a dark solid. It was collected by filtration, washed with ice-cold H_2O, cold acetone and diethyl ether, vacuum dried and purified *via* column chromatography.

*2.1.3. [Ru(Cl-Ph-tpy)(en)Cl]Cl (**1**)*

100.0 mg (0.181 mmol) of **P1**, 13.9 µL (0.218 mmol) of en, 76.9 mg (1.814 mmol) of LiCl and 75.9 µL (0.544 mmol) of Et_3N in 20 mL of ethanol/H_2O afforded **1** as a dark purple solid. The product was purified *via* column chromatography on alumina using dichloromethane/methanol (95 : 5, v/v) as eluent. The purple fraction was collected and the solvent removed to give a purple solid. Yield: 46.7 mg (44.7%). Anal Calcd for $C_{23}H_{22}Cl_3N_5Ru$ (575.88): C, 47.97; H, 3.85; N, 12.16. Found: C, 47.89; H, 3.93; N, 12.07. Complex **1** is soluble in water, methanol and ethanol, slightly soluble in acetonitrile, whereas it is insoluble in acetone, chloroform and dichloromethane. ^{1}H NMR (CD_3CN): 8.88 (d, 2H, *J* = 5.6 Hz, C6*H*/C6"*H*), 8.57 (s, 2H, C3'*H*/C5'*H*), 8.51 (d, 2H, *J* = 8.1 Hz, C3*H*/C3"*H*), 8.04 (d, 2H, *J* = 8.5 Hz, $C_AH/C_{A'}H$), 8.00 (t, 2H, C4*H*/C4"*H*), 7.65 (m, 4H, C5*H*/C5"*H*, $C_BH/C_{B'}H$), 5.37 (m br, 2H, NH_2 en), 3.26 (m, 2H, CH_2 en), the other two (i.e. CH_2 and NH_2) peaks of en

resonate at *ca*. 2.38 and *ca*. 2.01, and are overlapped with the HOD and CH_3CN resonances. Selected IR (KBr, cm^{-1}): ν_{CH2} 2923 (m), 2850 (m); ν_{tpy} 1578 (vs), 1472 (m), 1408 (s), 1089 (vs), 785 (s), 651 (w). UV/visible spectrum (H_2O; λ_{max}, nm (ε, M^{-1} cm^{-1})): 285 (37196), 319 (28920), 485 (6826).

*2.1.4. [Ru(Cl-Ph-tpy)(dach)Cl]Cl (**2**)*

100.0 mg (0.181 mmol) of **P1**, 26.1 μL (0.218 mmol) of dach, 76.9 mg (1.814 mmol) of LiCl and 75.9 μL (0.544 mmol) of Et_3N in 20 mL of ethanol/H_2O (3:1) afforded **2** as a dark purple solid. The product was purified *via* column chromatography on silica gel using dichloromethane/methanol (85 : 15, v/v) as eluent. The purple fraction was collected and the solvent removed to give a purple solid. Yield: 72.4 mg (63.4%). Anal Calcd for $C_{27}H_{28}Cl_3N_5Ru$ (629.97): C, 51.5; H, 4.48; N, 11.12. Found: C, 51.4; H, 4.42; N, 11.20. Complex **2** is soluble in water, methanol, ethanol and acetone, partially soluble in acetonitrile, whereas it is insoluble in chloroform and dichloromethane. ^{1}H NMR (CD_3CN): 9.04 (d, 1H, *J* = 5.4 Hz, C6*H*), 8.96 (d, 1H, *J* = 5.4 Hz, C6"*H*), 8.45 (s,1H, C3'*H*), 8.43 (s, 1H, C5'*H*), 8.37 (t br, 2H, C3*H*/C3"*H*), 7.98 (d, 2H, *J* = 8.5 Hz, $C_AH/C_{A'}H$), 7.87 (t, 2H, *J* = 7.6 Hz, C4*H*/C4"*H*), 7.62 (m br, 2H, C5*H*/C5"*H*), 7.49 (d, 2H, *J* = 8.5 Hz, $C_BH/C_{B'}H$), 5.86 (d, 1H, *J* = 12.0 Hz, N*H* dach), 5.06 (t, 1H, *J* = 11.9 Hz, N*H* dach), 2.71 – 2.62 (m, 1H, N*H* dach), 2.62 – 2.55 (m, 1H, C*H* dach), 2.12 – 1.88 (m, 2H, N*H* + C*H* dach), 1.87 – 1.71 (m, 2H, C*H* dach), 1.51 (t, 2H, *J* = 12.6 Hz, C*H* dach), 1.23 (m, 2H, C*H* dach), 1.11 (m, 1H, C*H* dach), 0.88 (m, 1H, C*H* dach). Selected IR (KBr, cm^{-1}): ν_{NH} 3133 (m); ν_{tpy} 1600 (s), 1473 (s), 1430 (s), 1088 (vs), 786 (vs), 652 (w). UV/visible spectrum (H_2O; λ_{max}, nm (ε, M^{-1} cm^{-1})): 285 (48050), 319 (38043), 492 (13932).

*2.1.5. [Ru(Cl-Ph-tpy)(bpy)Cl]Cl (**3**)*

100.0 mg (0.181 mmol) of **P1**, 34.0 mg, (0.218 mmol) of bpy, 76.9 mg (1.814 mmol) of LiCl and 75.9 µL (0.544 mmol) of Et_3N in 20 mL of ethanol/H_2O afforded **3** as a dark red crystalline solid. Yield: 106.5 mg (87.4%). Anal Calcd for $C_{31}H_{22}Cl_3N_5Ru$ (671.97): C, 55.41; H, 3.30; N, 10.42. Found: C, 55.40; H, 3.38; N, 10.40. Complex **3** is soluble in water, methanol, ethanol, acetone and acetonitrile, and partially soluble in chloroform and dichloromethane. ^{1}H NMR (D_2O): 9.55 (d, 1H, *J* = 5.6 Hz, Ca*H*), 8.82 (s, 2H, C3'*H*/C5'*H*), 8.67 (d, 1H, *J* = 8.2 Hz, Cd*H*), 8.52 (d, 2H, *J* = 8.1 Hz, C3*H*/C3"*H*), 8.36 – 8.26 (m, 2H, Cg*H*/Cc*H*), 8.03 (m, 3H, Cb*H*/C_AH/$C_{A'}H$), 7.97 (t, 2H, *J* = 7.9 Hz, C4*H*/C4"*H*), 7.81 (d, 2H, *J* = 5.6 Hz, C6*H*/C6"*H*), 7.72 (d, 2H, *J* = 8.1 Hz, C_BH/$C_{B'}H$), 7.67 (t, 1H, *J* = 7.8 Hz, Ch*H*), 7.38 – 7.28 (m, 3H, Cj*H*/C5*H*/C5"*H*), 6.92 (t, 1H, *J* = 6.7 Hz, Ci*H*). ^{1}H NMR (CD_3CN): 10.23 (d, 1H, *J* = 5.4 Hz, Ca*H*), 8.73 (s, 2H, C3'*H*/C5'*H*), 8.62 (d, 1H, *J* = 7.9 Hz, Cd*H*), 8.51 (d, 2H, *J* = 7.30 Hz, C3*H*/C3"*H*), 8.33 (d, 1H, *J* = 7.9 Hz, Cg*H*), 8.27 (m, 2H, Cc*H*), 8.10 (d, 2H, *J* = 8.3 Hz, C_AH/$C_{A'}H$), 7.98 (m, 1H, Cb*H*), 7.87 (t, 2H, *J* = 7.7 Hz, C4*H*/C4"*H*), 7.69 – 7.64 (m, 5H, Ch*H*/C6*H*/C6"*H*/C_BH/$C_{B'}H$), 7.31 (d, 1H, *J* = 5.7 Hz, Cj*H*) 7.27 (m, 2H, C5*H*/C5"*H*), 6.94 (t, 1H, *J* = 6.6 Hz, Ci*H*). Selected IR (KBr, cm^{-1}): ν_{tpy} 3058 (m), 1599 (s), 1455 (s), 1429 (s), 1091 (s), 790 (vs), 653 (m). UV/visible spectrum (H_2O; λ_{max}, nm (ε, M^{-1} cm^{-1})): 286 (57473), 315 (35855), 489 (12794).

2.2. Kinetic analysis

The hydrolysis kinetics of the complexes **1** and **2** were studied by stop-flow UV-Vis spectrophotometry by following the change in absorbance at specific wavelengths as a function of time. The working wavelength of each reaction corresponded to that of a maximum change in absorption derived from the difference spectra. The samples (0.1 mM) for the aquation studies, performed at 298 K, were prepared in distilled H_2O. The

absorption/time data for each complex were computer-fitted to the *pseudo*-first-order rate equation (Eq. 1), which gave the k_{obs} value (k) for each aquation process:

$$A=C_0 + C_1e^{-kt} \quad (1)$$

C_0 and C_1 are computer-fitted constants, and A is the absorbance at time t.

All kinetic data were computer-fitted using the programs Microsoft Excel 2007 and Origin 8.

2.3. DNA-binding studies

2.3.1. Absorption spectroscopic studies

The interaction of complexes **1** – **3** with CT DNA was studied, using UV-Vis spectroscopy, in order to investigate the possible binding modes to CT DNA and to calculate the binding constants (K_b). The DNA-binding experiments were performed at 37 °C. Buffered solution (5 mM tris(hydroxymethyl)aminomethane (Tris)-HCl, 50 mM NaCl, pH = 7.4) was used for the absorption measurements. A series of complex–DNA solutions were prepared by mixing complex solutions of fixed concentration (12.5 μM) with increments of the DNA stock solution (2.0 mM).

2.3.2. Fluorescence quenching measurements

The binding interaction of the complexes with DNA was also studied by fluorescence spectroscopy. The fluorescence intensities were measured with the excitation wavelength set at 527 nm and the fluorescence emission at 612 nm. The excitation and emission slit widths (each 10 nm) and scan rate were maintained constant for all the experiments. Stock solutions of DNA (2.0 mM) and complexes (0.1 mM) were prepared in 5 mM Tris-HCl buffer (pH = 7.4, 50 mM NaCl). A series of complex-DNA solutions were prepared by mixing DNA solutions with different concentration of complexes. For fluorescence determination, the final DNA concentration was 80.0 μM, and the complex concentrations varied from 8.0 μM to

80.0 μM. Before measurements, the system was shook and incubated at room temperature for 5 min. The emission was recorded at 550–750 nm.

2.3.3. Viscosity measurements

The viscosity of a DNA solution was measured in the presence of increasing amounts of complexes **1** – **3**. The flow time was measured with a digital stopwatch, each sample was measured three times, and then the average flow time was calculated. The data were presented as $(\eta/\eta_0)^{1/3}$ against *r*, where η is the viscosity of DNA in the presence of complex and η_0 is the viscosity of DNA alone in the buffered solution. The viscosity values were calculated from the observed flow time of the DNA-containing solutions (t) corrected for the flow time of the buffer alone (t_0), $\eta = (t-t_0)/t_0$.

2.4. Albumin-binding studies

The protein binding study was performed by tryptophan fluorescence quenching experiments using bovine serum albumin (BSA, 2 μM) in buffered solutions (containing 5 mM Tris and 50 mM NaCl at pH 7.4). Quenching of the emission intensity of tryptophan residues of BSA at 352 nm was monitored using the complexes **1 − 3** as quenchers with increasing concentration (up to 3.0×10^{-5} M) [17]. Fluorescence spectra were recorded in the range 300 − 500 nm at an excitation wavelength of 295 nm. The fluorescence spectra of the compounds in buffered solutions were recorded under the same experimental conditions, and no fluorescence emission was detected. The Stern−Volmer and Scatchard equations (Supporting Information, Eqs. S3−S6) and graphs have been used to study the interaction of the complexes with serum albumin and to calculate the corresponding constants [17].

2.5. Lipophilicity assay

Log $P_{o/w}$ is the partition coefficient between octanol and water which is determined using the flask-shaking method [18]. An aliquot of a stock solution of complexes **1 – 3** in 100 mM aqueous NaCl (0.9 % w/v to prevent aqueous interaction and remain saturated with octanol) was added to an equal volume of octanol (saturated with 0.9 % NaCl w/v). The mixture was shaken overnight at 60 rpm at 298 K to allow partitioning. After standing, the aqueous layer was carefully separated from the octanol layer for ruthenium analysis. The ruthenium concentration in the aqueous phase was determined using UV-Vis spectrophotometry and used to calculate the $[Ru]_o/[Ru]_w$ ratio.

2.6. Cell culture

Human cervix carcinoma cells (HeLa), human lung carcinoma cells (A549), and human fetal lung fibroblast cells (MRC-5) were maintained as monolayer culture in the Roswell Park Memorial Institute (RPMI) 1640 nutrient medium (Sigma Chemicals Co, USA). RPMI 1640 nutrient medium was prepared in sterile ionized water, supplemented with penicillin (192 IU/mL), streptomycin (200 mg/mL), 4-(2-hydroxyethyl)piperazine-1-ethanesulfonic acid (HEPES) (25 mM), L-glutamine (3 mM) and 10% of heat-inactivated fetal calf serum (FCS) (pH 7.2). The cells were grown at 37 °C in a humidified atmosphere of 95% air and 5% CO_2.

2.7. Cytotoxicity assay (MTT test)

The cytotoxicity of complexes **1 – 6**, and precursor **P1** was determined using 3-(4,5-dymethylthiazol-yl)-2,5-diphenyltetrazolium bromide (MTT, Sigma) assay as described previously. Briefly, cells were seeded into 96-well cell culture plates (Thermo Scientific Nunc™), at an appropriate cell density for each cell line. After 24 h of growth, cells were exposed to the investigated ruthenium complexes. The investigated complexes were

dissolved in DMSO at concentration of 10 mM and sequential dilutions were made in culture medium until to reach the desired concentrations. Final concentration of DMSO never exceeded 1% (v/v). After incubation periods of 72 h, 20 μL of MTT solution (5 mg/mL in phosphate buffer, pH 7.2) was added to each well. Samples were incubated for 4 h at 37 °C in humidified atmosphere of 5% CO_2, and then 100 μL of 10% sodium dodecyl sulfate (SDS) was added. Absorbance was recorded after 24 h, on an enzyme linked immunosorbent assay (ELISA) reader (Thermo Labsystems Multiskan EX 200-240 V), at the wavelength of 570 nm. The IC_{50} value, defined as the concentration of the compound causing 50% cell growth inhibition, was determined from the cell survival diagram.

2.8. Cell cycle analysis

Quantitative analysis of cell cycle phase distribution was performed by flow cytometric analysis of the DNA content in fixed HeLa and A549 cells, after staining with propidium iodide (PI) [19]. Cells were seeded at density of 2×10^5 cells /well at 6-well plate and growth in nutrition medium. After 24 h, cells were continually exposed to complex **3** or cisplatin. Control cells were incubated only in nutrient medium. After continual treatment, cells were collected by trypsinization, washed twice with ice-cold PBS, and fixed for 30 min in 70% EtOH. After fixation, cells were washed again with PBS and incubated with RNaseA (1 mg/mL) for 30 min at 37°C. Cells were than stained with PI (at concentration of 400 μg/mL) for 15 min before flow cytometric analysis. Cell cycle phase distribution was analyzed using a fluorescence activated sorting cells (FASC) Calibur Becton Dickinson flow cytometer and Cell Quest computer software.

3. Results and discussion

3.1. Synthesis and characterization

Treatment of the neutral Ru(III) precursor *mer*-[Ru(Cl-Ph-tpy)Cl_3] (**P1**) with a neutral *N-N* chelating ligand, such as en, dach or bpy, in the presence of triethylamine (Et_3N) and excess of LiCl afforded the cationic Ru(II) complexes [Ru(Cl-Ph-tpy)(*N-N*)Cl]Cl (*N-N* = en (**1**), dach (**2**) and bpy (**3**)) in good yields. All new complexes were characterized by NMR, IR and UV-Vis spectroscopy, and elemental analysis. Crystals of [Ru(Cl-Ph-tpy)(en)Cl]Cl (**1**) were obtained, and the structure was partially solved by X-ray crystallography which confirmed the proposed structure (Fig. S1 in the SI). However, it could not be adequately refined because of the low crystal quality, and thus no crystal data are reported for the analysis. In the obtained structure of the complex cation, the Ru ion displays the typical octahedral geometry with the tridentate Cl-Ph-tpy ligand coordinated with the expected meridional geometry, the en acting as chelating ligand, whereas the sixth coordination site is occupied by a chloride ion.

The ^{1}H spectrum of **1** in CD_3CN is consistent with a *Cs* symmetry in solution due to the conformational mobility of the en backbone that averages it to a planar ligand. In the ^{1}H spectrum there are seven aromatic resonances assigned to the two equal halves of the Cl-Ph-tpy and two upfield peaks attributed to the equatorial half fragment (CH_2 and NH_2) of the en ligand (Fig. S2). The two en resonances of the axial fragment, which fall into the shielding cone of the adjacent Cl-Ph-tpy ligand and thus they are remarkably shifted upfield, are overlapped with the intense broad CD_3CN peaks.

Conversely, the ^{1}H NMR spectrum of **2** in CD_3CN is more complicated due to the conformational rigidity of coordinated dach [20,21] that removes the mirror plane bisecting the Cl-Ph-tpy ligand in **1**. Thus, in the ^{1}H NMR spectrum the resonances of the corresponding protons of the two halves of Cl-Ph-tpy are partially overlapped except for H6/H6" (two doublets at δ = 9.04 and 8.96) and H3'/H5' (two singlets at δ = 8.45 and 8.37), which are well resolved (Fig. S3).

The ^{1}H NMR spectrum of **3** in CD_3CN is consistent with the symmetry of the complex: seven resonances attributed to the symmetric Cl-Ph-tpy ligand and eight multiplets assigned to the two inequivalent halves of bpy (Fig. 2). It is worth noting that each peak of the axial bpy ring is remarkably shifted upfield compared to that of the corresponding proton on the other ring (e.g. δHi = 6.94 *vs*. δHb = 7.98) due to the shielding effect of Cl-Ph-tpy. Correspondingly, the protons of the terminal aromatic rings of Cl-Ph-tpy are affected by the shielding cone of bpy and thus their resonances are also remarkably upfield shifted; in particular the H6/H6" protons resonate at 7.67 ppm, that is *ca*. 1.00 ppm more upfield compared to those of **1** and **2**.

Fig. 2.

The solid state IR spectra of complexes **1 – 3** show the typical bands of the terpyridine ligands: the aromatic C–H stretching in the region 3060 – 2850 cm^{-1}, and the most characteristic strong band in the region 1395 – 1616 cm^{-1} assigned to ν(C=N) and ν(C=C) stretching [22,23]. The band at 1011 cm^{-1}, present in the spectra of all complexes, results from the ring breathing modes of the individual pyridine rings [11,24].

The solution electronic absorption spectra of complexes **1 – 3** exhibited several intense bands in the UV region ($200 < \lambda < 330$ nm), attributed to intra-ligand ($\pi \rightarrow \pi^*$) charge transfer transitions, and a broad intense band (with an unresolved shoulder) in the visible region attributed to metal to ligand $d\pi(Ru) \rightarrow \pi^*$(polypyridyl) charge transfer (MLCT) transitions [11,22,25-28].

3.2. Chemical behavior in aqueous solution

The chemical behavior of the new complexes in aqueous solution was first investigated qualitatively by NMR spectroscopy in view of their potential reactivity towards biological (macro)molecules, such as proteins, DNA etc. The chloride ligand in the cationic complexes **1** and **2** turned out to be very labile in aqueous solution. After dissolution in D_2O, a new set of resonances was observed to grow both in the aromatic (Cl-Ph-tpy resonances) and in the upfield (en or dach resonances) regions of the ^{1}H NMR spectra. These new resonances, which grew at the expense of those of the parent compound, were attributed to the aqua species $[Ru(Cl\text{-}Ph\text{-}tpy)(en)(H_2O)]^{2+}$ (**1aq**) and $[Ru(Cl\text{-}Ph\text{-}tpy)(dach)(H_2O)]^{2+}$ (**2aq**), respectively (Scheme 1). According to integration, *ca.* 50% of complex **1** is already aquated 10 min after dissolution, and the system reached equilibrium within *ca*. 1 h with 1:9 ratio between **1** and **1aq** (Fig. S4). The chemical behavior in aqueous solution of the dach derivative **2** is very similar to that described for **1** (Fig. S5). Contrary to **1** and **2**, the bpy complex **3** release the Cl^- ligand, yielding the aqua species $[Ru(Cl\text{-}Ph\text{-}tpy)(bpy)(H_2O)]^{2+}$ (**3aq**) at a much slower rate, but to a comparable extent (Fig. S6). The equilibrium was reached *ca*. 24 h after dissolution. The greater lability of the Cl^- ligand in compounds **1** and **2** is attributed to the stronger *trans* influence of the pure σ-donor ligands en and dach, respectively, compared to the (also) π-acceptor bpy in compound **3**. Interestingly, no release of the *N*-*N* ligand was detected from all complexes during the observation times. Addition of a large excess of NaCl (*ca*. 1.00 M) into the equilibrated solution of **1aq – 3aq** induced rapid precipitation of the chlorido derivatives **1 – 3**.

Scheme 1.

3.3. UV-Vis kinetics of aquation

The kinetics of aquation of complexes **1** and **2** were quantitatively studied by UV-Vis spectroscopy at 298 K on 0.1 mM solutions. Complex **3** was excluded from these studies because, according to the NMR evidences, it hydrolyzes the Cl ligand at a very slow rate. The rapid reversion of the equilibrium and the precipitation of the complexes upon addition of NaCl prohibited anation kinetics studies and, therefore, the calculation of the equilibrium constants K_{aq}.

The UV-Vis spectra of complexes **1** and **2** show significant time-dependent changes in the region 200 – 800 nm (Fig. S7) with clean isosbestic points that, consistent with the NMR observation, suggest the occurrence of a single hydrolytic process (i.e. conversion of the initial chlorido complex into the corresponding aqua species **1aq** and **2aq**, respectively). The wavelength corresponding to the maximum change in absorption (Fig. S7, difference spectra) was selected for the kinetic studies (470 nm for **1** and 471 nm for **2**). In each case the time course of the absorbance followed *pseudo*-first-order kinetics (Fig. 3) that afforded the rate constants k_{obs} listed in Table 1. It can be seen that both complexes hydrolyze at a similar rate, $k_{obs} = 6.10 \times 10^{-3}$ s^{-1} for **1** and 4.90×10^{-3} s^{-1} for **2**, respectively. Complexes **1** and **2** hydrolyze slightly faster than their Ru-tpy analogues [Ru(Cl-tpy)(en)Cl]Cl (**4**) and [Ru(Cl-tpy)(dach)Cl]Cl (**5**) ($2.52 – 3.94 \times 10^{-3}$ s^{-1}) [6], and *ca*. two orders of magnitude higher than those of the established anticancer drug cisplatin (6.32×10^{-5} and 2.5×10^{-5} s^{-1} for the first and second aquation process, respectively) [29]. These results imply that our coordination compounds evolve to the active aqua species much faster than cisplatin in low chloride concentration environments corresponding to intracellular conditions. However, it has been proved that fast aquation of complexes might lead to reduced activity and/or to increased toxicity due to their fast binding to biomolecules other than those responsible for tumor proliferation such as DNA.

Fig. 3.

Table 1. Rate constants for the aquation and half-lives at 298 K in H_2O for compounds **1** and **2**.

3.4. DNA-binding studies

DNA is a critical therapeutic target that is responsible for, and the focus of, a wide variety of intracellular interactions [30-34]. Many ruthenium(II) polypyridyl complexes are well-established DNA intercalators with useful spectroscopic properties and relatively low toxicity [35] which makes them ideal diagnostic agents [36]. On the other hand, the most of ruthenium(II) complexes that contain a labile ligand (such as Cl^-), can bind covalently, after hydrolysis, to DNA through guanine *N*7 [37]. In our previous work, we revealed that the Ru(II)-tpy complexes **4 – 6** both intercalate and covalently bind to CT DNA [7]. The combination of these modes of interaction can be utilized to improve the binding affinity and selectivity of ruthenium complexes. The aim of this study was to investigate the effect of the phenyl-substituent on the terpyridyl ligand and of the nature of the inert chelating ligands on the binding mode of Ru(II)-polypyridyl complexes to DNA and to relate this to the differences in their anticancer activity.

3.4.1. Absorption spectroscopic studies

The application of electronic absorption spectroscopy is one of the most universally employed methods for the determination of the binding modes and binding extent of metal complexes with DNA. The absorption intensity of the complexes may decrease (hypochromism) or increase (hyperchromism) with a slight increase in the absorption wavelength (bathochromism) upon addition of DNA.

The UV-Vis spectra were recorded for a constant concentration of the complexes at different [complex]:[DNA] mixing ratios (r). The UV-Vis spectra of complexes **1 – 3** in the absence and presence of CT DNA are given in Fig. S8. The increase in the intensity at the MLCT band for all three complexes indicated that the interaction with CT DNA resulted in the direct formation of a new complex with double-helical CT DNA. In the UV-Vis spectrum of complex **1**, the two bands at 422 and 488 nm, present a hyperchromism upon addition of increasing amounts of CT DNA (Fig. S8), suggesting the tight binding to CT DNA. Additionally, the band at 422 nm presents a red shift (bathochromism) of 6 nm (up to 428 nm), suggesting the stabilization of the CT DNA duplex [17,38]. The behavior of complex **2** was quite similar (the band centered at 496 nm presents a hyperchromism) upon addition of increasing amounts of CT DNA (Fig. S8). The band at 424 nm exhibits a hyperchromism accompanied by a 4 nm red shift (to 428 nm). Similarly, in the UV-Vis spectrum of complex **3**, the two bands at 315 and 490 nm exhibit a hyperchromism upon addition of CT DNA (Fig. S8).

The above results suggest that all complexes can bind to CT DNA and stabilize the CT DNA duplex, although the exact mode of binding cannot be reliably proposed on the basis of UV-Vis spectroscopic studies [17,38]. It is important to emphasize that the studied complexes contain both a leaving group and a DNA intercalating ligand, and hence, they could interact with DNA in a bifunctional mode, including covalent binding to the nucleobases and non-covalent intercalation.

The intrinsic binding constants K_b of complexes **1 – 3**, calculated by the equation (S1) and the plots (Fig. S9), were $(1.0 \pm 0.2) \times 10^6$ M^{-1}, $(2.8 \pm 0.1) \times 10^6$ M^{-1} and $(9.0 \pm 0.2) \times 10^6$ M^{-1}, respectively (Table 2). The K_b values suggest a strong binding of the complexes to CT DNA, with complex **3** exhibiting higher K_b values compared to complexes **1** and **2**. For comparison, the polypyridyl compounds **4 – 6** that are believed to bind to DNA in a

bifunctional manner (covalently and non-covalently), have K_b values (2.1 – 10.0 x 10^4 M^{-1}) [7] that are *ca*. from one to two orders of magnitude lower than those of complexes **1 – 3**, respectively, implying that the introduction of the chlorophenyl fragment in the tpy ligand has a significant effect on the DNA binding activity. Changing the overall nature (electron-donating or -withdrawing) of the substituents on the tpy moiety affects the π-back-donation ability of the ligand and hence the electrophilicity of the metal centre. The chlorophenyl-substitution on the 4'-position of tpy has a strong electron-withdrawing effect on the tpy ligand and, consequently, on the metal center. This results in an increase of the reactivity of the ruthenium complexes **1 – 3**. Furthermore, the K_b values of **1 – 3** are higher than that of the classical intercalator EB, which has a binding affinity for CT DNA of 1.23 (± 0.07) × 10^5 M^{-1} [17,38,39].

Table 2. The DNA-binding constants (K_b) and Stern–Volmer constants (V, K_{sv}) from EB–DNA fluorescence for **1** – **3**.

3.4.2. Fluorescence quenching studies

Ethidium bromide (EB) is a classical intercalator that gives significant fluorescence emission intensity when it intercalates into the base pairs of DNA. When it is replaced or excluded from the internal hydrophobic environment of the DNA double helix by other small molecules, its fluorescence emission is effectively quenched by external polar solvent molecules such as H_2O [40]. Compounds **1 – 3** do not show any significant fluorescence at room temperature in solution or in the presence of CT DNA, when excited at 527 nm. Furthermore, the addition of complexes **1 – 3** to a solution containing EB does not provoke quenching of free EB fluorescence, and no new peaks appear in the spectra. The changes observed in the spectra of EB on its binding to CT DNA are often used for studying the DNA

binding activity of metal complexes, since the addition of a compound, capable of intercalating DNA equally or more strongly than EB, could result in a quenching of the EB-DNA florescence emission.

The fluorescence quenching curves of EB bound to DNA in the absence and presence of the complexes are shown in Fig. 4. The addition of increasing amounts (up to r = 1.0) of complexes **1** – **3** resulted in significant decrease of the intensity of the emission band at 612 nm, indicating competition of the compounds with EB in binding to DNA (Fig. 4). The observed quenching of DNA–EB fluorescence suggests that they can displace EB from the DNA–EB complex and that they can probably interact with CT DNA by the intercalative mode [38,41,42].

Quenching mechanism can be predicted from Stern-Volmer plots. In the case of all three complexes **1 – 3**, the simple Stern–Volmer plots (I_0/I versus [Q]) showed an upward curvature (Eq. S2 and Fig. 4) which is obtained when both static and dynamic quenching occur. The static quenching constant *V* was obtained from the modified form of the Stern-Volmer equation (Eq. S3) by plotting $I_0/Ie^{V[Q]}$ versus [Q] by varying *V* until a linear plot was obtained. The highest value of correlation coefficient was used as criterion for linearity of the plot to obtain a precise value of *V*. The (dynamic) collisional quenching constant, K_{sv} was then obtained from the slope of the linear plots (Fig. S10). The *V* and K_{sv} values so obtained are given in Table 2. All three complexes showed high values of the quenching constant indicating their great efficiency to replace EB and bind strongly to DNA, which is in agreement with the high values of their DNA binding constant (K_b). These additional interactions could contribute to the unique binding modes to duplex DNA and induce different structural distortions in DNA compared to cisplatin. Similar observations were reported by Sadler and coworkers for the promising antitumor group of organoruthenium(II) complexes where the direct coordinative binding of the monofunctional [Ru(η^6-

biphenyl)(en)Cl]$^{+}$ complex to *N*7 of guanine bases in DNA was complemented by intercalative binding of the biphenyl ligand [43].

Fig. 4.

3.4.3. Viscosity measurements

In order to further confirm the modes of binding of complexes **1** – **3** to CT DNA, viscosity measurements of DNA solutions were performed in the presence and absence of these complexes. The viscosity of DNA is sensitive to length changes and is regarded as the least ambiguous and the most critical clues of the DNA binding mode in solution [44,45]. The addition of increasing amounts (up to r = 1.0) of complexes **1** – **3** to a DNA solution (0.01 mM) resulted in an increase in the relative viscosity of DNA (Fig. S11), which was more pronounced upon addition of complex **2**. In the case of classic intercalation, DNA base pairs are separated to host the bound compound resulting in increased DNA viscosity, the magnitude of which is usually in accordance to the strength of the interaction, because of the lengthening of the DNA helix. Therefore, the observed viscosity increase may be explained by an increase in the overall DNA length provoked by the insertion of the compounds in between the DNA base pairs due to interaction *via* intercalation through the aromatic chromophore of Cl-Ph-tpy and bpy ligands in the complexes. Additionally, these observations are in substantial agreement with the previously obtained results for the Cl-tpy complexes **4** and **5** [7].

3.5. Albumin-binding studies

Serum albumin, as the most abundant protein in the blood circulatory system, plays important role in the transport and delivery of many pharmaceuticals to the sites of disease [46]. Therefore, studies on the binding of biologically active compounds with proteins not

only provide useful information on the structural features that determine the therapeutic effectiveness of drugs, but is also important for studying the pharmacological response of drugs and design of dosage forms. Interactions of metallodrugs with proteins are crucial for their biodistribution, toxicity, and even for their mechanism of action [47]. Furthermore, binding of drugs to proteins may affect (either enhance or reduce) the biological properties of the original drug.

We have recently shown, by means of UV-Vis and ^{1}H NMR spectroscopies supported by DFT calculations, as well as by liquid chromatography (LC) and inductively coupled plasma optical emission spectrometry (ICP-OES), that complexes **4** and **5** coordinate to BSA through the nitrogen atom of imidazole ring of several histidine (His) residues [7,8]. The binding mechanism involved the dissociation of the chloride ligand and its replacement by a water molecule, prior to binding to His. In this study, the interaction between BSA and complexes **1 – 3** was investigated by florescence spectroscopy as this method allows a quantitative assessment of the binding strength.

BSA is the most extensively studied serum albumin because of its high structural homology with HSA (human serum albumin). HSA contains one tryptophan located at position 214, while BSA has two tryptophan residues, Trp-134 and Trp-212. BSA solution exhibits an intense fluorescence emission with $\lambda_{em,max}$ = 352 nm, when excited at 295 nm [48]. The changes and the quenching observed in the fluorescence emission spectra of tryptophan in BSA upon addition of complexes are primarily due to changes in protein conformation, subunit association, substrate binding, or denaturation.

Addition of the complexes **1 – 3** to a BSA solution (up to *r* values of 15) results in a significant quenching of BSA fluorescence at λ = 352 nm for **2** and **3**, and moderate quenching for complex **1** (Fig. 5 and Fig. S12). The observed quenching may be attributed to changes in protein tertiary structure leading to changes in tryptophan environment of BSA,

and thus indicating the binding of each complex to the albumin [48-50]. Furthermore, the maximum of the bands were slightly shifted from 352 to 355, 356 or 359 nm, for **1**, **2** and **3**, respectively (Fig. S12). The red shift implies the formation of ruthenated BSA adducts, which altered the polarity of microenvironment in the vicinity of tryptophan.

In the case of all three complexes **1 – 3**, the simple Stern–Volmer plots (I_0/I versus [Q]) showed an upward curvature (Eqs. S4, S5 and Fig. S13). The static quenching constant *V* was obtained from the modified form of the Stern-Volmer equation (Eq. S6) by plotting $I_0/Ie^{V[Q]}$ versus [Q] by varying *V* until a linear plot was obtained. The highest value of correlation coefficient was used as criterion for linearity of the plot to obtain a precise value of *V*. The (dynamic) collisional quenching constant, K_{sv} was then obtained from the slope of the linear plots (inset Fig. S13). The *V* and K_{sv} values so obtained are given in Table 3. The magnitude of static quenching constant was smaller than the collisional quenching constant, but both were of the order of 10^4.

The quenching rate constant (k_q) depends on the probability of a collision between fluorophore and quencher and is a measure of the exposure of tryptophan residues to the drug. The k_q values are also given in Table 3 and indicate good quenching ability of the BSA fluorescence, with **2** exhibiting the highest k_q value ($k_q = 4.6 \pm (0.5) \times 10^{12}$ M^{-1} s^{-1}). The upper limit of k_q expected for a diffusion-controlled bimolecular process is 10^{10} M^{-1} s^{-1}. The high magnitude of k_q in the present study (10^{12} M^{-1} s^{-1}) shows that the process is not entirely diffusion controlled, specific drug-protein interactions are also involved which make k_q larger [48-50].

The values of the BSA-binding constant (*K*) and the number of binding sites per albumin (n), as calculated from the Scatchard equation (Eq. S7) and Scatchard plot (Fig. S14) for all compounds are given in Table 3. The highest binding constant to BSA is found for

complex **3**. The *n* values for the complexes **1 – 3** average out to be 1 which suggests that there is only one binding site available on the protein [51].

The analysis of the BSA-binding constants (*K*) is rather useful to infer how a molecular species, particularly a drug, will be distributed in blood plasma. All three complexes have *K* values that are within the range which could be considered optimal; they are high enough so that the compounds bind to BSA to get transport, but nevertheless they are sufficiently low (i.e., below the value of 10^{15} M^{-1}, which is the association constant of avidin with diverse ligands; this interaction is considered the strongest among known noncovalent interactions) so that the compounds can be released from the albumin upon arrival at the target cells [52-54]. This binding might provide a path to enhance the selectivity of **1 – 3** by passive targeting to tumor tissues through BSA binding.

Fig. 5.

Table 3. BSA constants and parameters (K_{sv}, k_q, *K*, *n* and *V*) derived for complexes **1 – 3**

3.6. Hydrophobicity measurements

Lipophilicity is one of the most important factors in pharmaceutical research and can be considered a key determinant of the pharmacokinetic properties of a drug and its interaction with macromolecular targets. Octanol–water partition coefficients (log $P_{o/w}$) provide a measure of drug lipophilicity, which indicates the ability of a molecule to pass through cell membranes [55]. Knowledge of the partition coefficient is valuable, and it is frequently used in structure-activity relationship (SAR) and quantitative structure-activity relationship (QSAR) studies. The lipophilicity of complexes **1 – 3** was determined by measuring the concentration ratio of the corresponding complex in the aqueous phase at

equilibrium state. After mixing with octanol and water, complexes **1** – **3** were distributed mostly in the octanol phase. All three complexes gave positive log $P_{o/w}$ values, showing them to be hydrophobic in nature. Complex **3** (0.39) tended to be more hydrophobic than **1** (0.27), and **2** (0.20), which may facilitate its cell uptake efficiency and enhance its anticancer activity.

3.7. In vitro cytotoxicity

The *in vitro* cytotoxicity of complexes **1 – 6**, and precursor **P1** against two selected human cancer cell lines (HeLa and A549) and one normal cell line (MRC-5) was determined by MTT assay. The widely used clinical chemotherapeutic agent cisplatin was used as a positive control. Activity was determined after incubation with investigated complexes for 72 h (Fig. 6). From Table 4, it is clear that complex **3** is generally the most active and exhibits low IC_{50} values of 12.7 μM for HeLa cells, and 4 times higher IC_{50} values (*ca.* 53.8 μM) for A549 cell line. Complexes **1** and **2** show moderate *in vitro* cytotoxicity against the HeLa cell line with an IC_{50} of *ca*. 84.8 and 96.3 μM, respectively, *i.e.* from about 7 to 8 times lower activity than that of the most potent bpy complex **3**. Conversely, **1** and **2** do not show any activity against A549 cell line. All three complexes reveal a remarkable selectivity towards the human cervix carcinoma cells (HeLa). In addition, the previously described Cl-tpy compounds [Ru(Cl-tpy)(dach)Cl]Cl (**5**) and [Ru(Cl-tpy)(bpy)Cl]Cl (**6**) [7], show lower activity in comparison with their Cl-Ph-tpy analogues **2** and **3**, respectively. Interestingly, whereas in the series of the Cl-Ph-tpy compounds **1** – **3** the bpy complex **3** is the most active, in the series of the Cl-tpy compounds **4** – **6** the en complex **4** is the uppermost. These results indicate that the biological activity of Ru(II) polypyridyl complexes depends on the nature of the meridional tridentate ligand. The introduction of chlorophenyl-substituent in the tpy ligand results in an increase in the anticancer activity. In addition, the presence of bipyridine

in the coordination sphere of the ruthenium(II) chlorophenyl-substituted tpy complexes is very important for the cytotoxic activity. Compared to the pure σ-donor ligands en and dach, the π-acceptor bpy may increase the electrophilicity of the metal center and hence the reactivity of ruthenium(II) complexes. On the other hand, the possibility of bpy intercalation between the DNA bases has also been recognized [56].

The *in vitro* activity of anticancer drugs can often be related in part, to their lipophilic character; higher hydrophobicity may contribute to an increased uptake of the complex by the cells, thereby enhancing the anticancer activity [57-60]. For example, complex **3** presents the highest lipophilicity and hence generates the strongest cytotoxicity. In contrast, complex **2** presents the lowest lipophilicity and therefore exhibits the weakest cytotoxicity. The most likely reason may be that it is easier for complex **3** to pass through the cell membrane, which induces a higher cell uptake and a higher cytotoxicity. All these findings further demonstrate that aromatic substituent on the tpy ligand has great influence on the biological activity of these complexes. Similar to Sadler and co-workers who have shown that there is a direct correlation between the lipophilicity of the arene ligand and cytotoxicity [61], in the present work we demonstrated that the cytotoxicity of the Ru-tpy complexes can be increased by using more lipophilic ligands.

Table 4. IC_{50} values for complexes **1 – 6** and precursor **P1** towards different cell lines in comparison to cisplatin, obtained from the MTT assay, after 72 h drug exposure. In all cases, the values represent the mean of three independent experiments.

Fig. 6.

3.8. Cell cycle analysis

The effect on cell cycle progression of HeLa and A549 cells after treatment with complex **3** was examined by flow cytometry, using staining with propidium iodide PI [19]. Complex **3** was selected among the other investigated complexes due to its promising profile: high cytotoxicity and selectivity toward HeLa cells, moderate cytotoxicity against A549 cells, and low cytotoxicity to normal cells (MRC-5). In comparison, the well-established drug cisplatin (CDDP) was investigated as well, under the same conditions.

The results of the cell cycle analysis of HeLa cells treated with **3**, presented in Figure 7, show that after 48 h of action with $2IC_{50}$ and $3IC_{50}$ concentrations (IC_{50} values determined for 72 h agent action) induced barely noticeable changes: slight decrease of percent of cells in G1 phase and slight increase of percent of cells in S and G2. Simultaneously, no change of percent of cells in Sub-G1 phase (hypodiploid cells), which is considered as a marker of cell death by apoptosis [62], was observed in studied conditions (Fig. 7). On the other hand, cisplatin induced decrease of percent of cells in G1 (up to 32.8 % compared to control 56.6 %) and increase of percent of cells in S phase (up to 51 % compared to control 18.9 %). Cisplatin S phase arrest that indicates block of DNA replication is in agreement with the literature concerning the mechanism of action of CDDP and its effect on the cell cycle [63,64]. Lack of cell cycle perturbations after complex **3** action indicate that its interactions with DNA, determined by DNA binding studies, are not crucial/decisive for its cytotoxicity and perhaps a different mechanism of action compared to that of cisplatin, is implicated for the obtained activity.

The cell cycle analysis of A549 cells after 48 h treatment with **3** (with concentrations corresponding to $2IC_{50}$ and $3IC_{50}$ determined for 72 h agent action), presented in Figure 8, show minor increase in percent of cells in G1 phase (up to 82.4 % compared to control 74.3 %) and decrease in S phase (up to 7.5 % compared to control 12.5 %). This may indicate the

presence of some type of interactions with DNA that prevent the entry of cells in the synthetic phase of cell cycle. Under the same experimental conditions, cisplatin induced tremendous perturbations of cell cycle after 48 h treatment (with $2IC_{50}$ and $3IC_{50}$ concentrations), with enormous decrease of percent of cells in G1 phase (up to 15.8 % compared to control 74.3 %) and accumulation of cells in S and G2/M phases of the cell cycle, in agreement with previously published results [65]. In terms of the results related to the mechanism of action of our ruthenium complex **3**, although the complicated nature of A549 cell line makes difficult the interpretation of the results with respect to cisplatin, it allows us to conclude that results of cell cycle analysis confirmed again different mode of interactions of **3**, compared to cisplatin, with DNA.

Fig. 7.

Fig. 8.

4. Conclusion

In a previous work we have reported the synthesis and extensive studies including thorough investigation on their stability and behavior in aqueous solution, DNA/BSA binding activity and *in vitro* antiproliferative activity, of a series of new Ru(II)-tpy complexes of the general formula [Ru(Cl-tpy)(*N*-*N*)Cl]Cl (where Cl-tpy = 4'-chloro-2,2':6',2''-terpyridine; *N*-*N* = en (**4**), dach (**5**) or bpy (**6**)) [6-8]. We found that these compounds, in particular complex **4**, show promising antitumor activity. With the aim of expanding the structure activity relationship investigation on these polypyridyl Ru(II) complexes, we were testing another meridional tridentate ligand. In that context, we described here the synthesis and structural characterization of a series of new monofunctional ruthenium(II) complexes of the general

formula *mer*-[Ru(Cl-Ph-tpy)(*N*-*N*)Cl]Cl (where *N*-*N* = en (**1**), dach (**2**) or bpy (**3**)), in which the Cl-tpy ligand was replaced by the chlorophenyl-substituted tpy ligand (Cl-Ph-tpy), while the rest of the coordination sphere remained unchanged. In view of their potential antitumor activity, their chemical behavior in aqueous solution was studied by UV-Vis and NMR spectroscopy and compared to that of the previously described analogues [Ru(Cl-tpy)(*N*-*N*)Cl]Cl. These studies showed that complexes **1 – 3** release the Cl^- ligand to form the corresponding aqua species. The rate of hydrolysis was found to depend markedly on the nature of the chelating ligand (minutes for en and dach, hours for bpy), but its extent was similar in all cases, with a *ca*. 1:9 ratio between intact and aquated species at equilibrium, at NMR concentrations.

UV-Vis spectroscopy studies and competitive binding studies with EB revealed the ability of the complexes to bind to CT DNA covalently and non-covalently through intercalation. All complexes show good binding affinity to BSA, with relatively high binding constants. The high *K* values observed for the complexes **1 – 3** suggest that these compounds can be efficiently stored and transported in the body by BSA. The cytotoxicity of **1 – 3** was evaluated against two different tumor cell lines (HeLa and A549), and one normal cell line (MRC-5) in comparison with their Cl-tpy analogues **4 – 6**, their respective precursor *mer*-[Ru(Cl-Ph-tpy)Cl_3] (**P1**) and cisplatin. Complex **3** displayed the highest cytotoxicity when tested on the HeLa cell line. Contrary to what observed for the corresponding Ru-tpy complexes **4 – 6**, that their cytotoxicity roughly correlates with their ability to hydrolyze the monodentate ligand at a reasonable rate, the most active bpy complex **3** hydrolyses slower than the other two complexes.

The present results clearly confirmed that the relatively rapid availability of one coordination position on the Ru center is not an essential requirement for observing anticancer activity, which is in contrary with the results obtained for the corresponding Ru-

tpy complexes, as well as with the results obtained by Sadler and Alessio for the organoruthenium(II) half-sandwich compounds and coordination Ru(II)-[9]aneS3 complexes, respectively [5,7,20]. In addition, we showed here that the presence of a chelating ligand that is unable of making hydrogen bonds, such as bpy, not necessarily induces the loss of cytotoxic activity. In fact, the bpy complex **3** was the most active. We speculate that the activity of such complexes is relevant to their hydrophobicity and their ability to open a coordination site. These two properties largely determine their mechanism of action: by increasing the aromaticity (*viz.* hydrophobicity), the intercalation is the predominant mechanism, whereas in less aromatic molecules the covalent binding. The lack of correlation between cell growth inhibition, DNA and BSA binding affinity and hydrolysis stability suggests that multiple targets and multiple mechanisms involve in the anticancer process of the compounds. These differences may play very important roles in their antitumor activity and could contribute to the different mechanism for cytotoxicity compared to cisplatin.

Abbreviations

Cl-Ph-tpy	4'-(chlorophenyl)-2,2':6',2'-terpyridine
en	1,2-diaminoethane
dach	1,2-diaminocyclohexane
bpy	2,2'-bipyridine
CT DNA	calf thymus DNA
EB	ethidium bromide
tpy	2,2':6',2"-terpyridine
Cl-tpy	4’-chloro-2,2':6',2"-terpyridine
RPMI	Roswell Park Memorial Institute
TRIS	tris(hydroxymethyl)aminomethane

DSS	2,2-dimethyl-2,2-silapentane-5-sulfonate
DMSO	dimethyl sulfoxide
HEPES	4-(2-hydroxymethyl)piperazine-1-ethansulfonic acid
FCS	fetal calf serum
MTT	3-(4,5-dimethylthiazol-yl)-2,5-diphenyltetrazolium bromide
SDS	sodium dodecyl sulfate
ELISA	enzyme linked immunosorbent assay
PI	propidium iodide
PBS	phosphate buffer saline
FACS	fluorescence activated sorting cells
LC	liquid chromatography
ICP-OES	inductively coupled plasma optical emission spectroscopy
His	histidine
CDDR	cisplatin

Acknowledgments

The authors gratefully acknowledge financial support from the Ministry of Education, Science and Technological Development of the Republic of Serbia, Project No. 172011.

References

[1] E. Alessio, Bioinorganic Medicinal Chemistry, Wiley-VCH Verlag & Co. KGaA, Weinheim, Germany, 2011.

[2] P.E.N. Barry, J.P. Sadler, Chem. Commun. 49 (2013) 5106–5131.

[3] R. Trondl, P. Heffeter, C.R. Kowol, M.A. Jakupec, W. Berger, B.K. Keppler, Chem. Sci. 5 (2014) 2925–2932.

[4] P.C. Bruijnincx, P.J. Sadler, J. Curr. Opin. Chem. Biol. 12 (2008) 197–206.

[5] Y.K. Yan, M. Melchart, A. Habtemariam, P.J. Sadler, Chem. Commun. (2005) 4764–4776.

[6] A. Rilak, I. Bratsos, E. Zangrando, J. Kljun, I. Turel, Ž.D. Bugarčić, E. Alessio, Inorg. Chem. 53 (2014) 6113–6126.

[7] D. Lazić, A. Arsenijević, R. Puchta, Ž.D. Bugarčić, A. Rilak, Dalton Trans. 45 (2016) 4633-4646.

[8] M. Nišavić, R. Masnikosa, A. Butorac, K. Perica, A. Rilak, A. Hozić, M. Petković, M. Cindrić, J. Inorg. Biochem. 159 (2016) 89–95.

[9] Li.-Feng. Tan, Xue.-Jiao. Chen, Jian.-Liang. Shen, Xi.-Ling. Liang, J. Chem. Sci. 121 (2009) 397–405.

[10] M.-Y. Ho, M.-L. Chiou, W.-S. Du, F. Y. Chang, Y.-J. Weng, C.-C. Cheng, J. Inorg. Biochem. 105 (2011) 902–910.

[11] M.N. Patel, D.S. Gandhi, P.A. Parmar, H.N. Joshi, J. Coord. Chem. 65 (2012) 1926–1936.

[12] A. Hofmann, D. Jaganyi, O.Q. Munro, G. Liehr, R. van Eldik, Inorg. Chem. 42 (2003) 1688–1700.

[13] D. Jaganyi. D. Reddy, J.A. Gertenbach, A. Hofmann, R. van Eldik, Dalton Trans. (2004) 299–304.

[14] J. Wang, Y.-Q. Fang, G.S. Hanan, F. Loiseau, S. Campagna, Inorg. Chem. Commun. 44 (2005) 5–7.

[15] D. Reddy, K.J. Akerman, M.P. Akerman, D. Jaganyi, Trans. Met. Chem. 36 (2011) 593–602.

[16] K.A. Meadows, F. Liu, J. Sou, B.P. Hudson, D.R. McMillin, Inorg. Chem. 32 (1993) 2919–2923.

[17] A. Tarushi, E. Polatoglou, J. Kljun, I. Turel, G. Psomas, D.P. Kessissoglou, Dalton. Trans. 40 (2011) 9461–9473.

[18] C.A. Puckett, J.K. Barton, J. Am. Chem. Soc. 129 (2007) 46-47.

[19] M.G. Ormerod, Analysis of DNA-General Methods. Flow Cytometry, a Practical Approach, Oxford University Press, New York, 1994, pp. 119–125.

[20] I. Bratsos, E. Mitri, F. Ravalico, E. Zangrando, T. Gianferrara, A. Bergamo, E. Alessio, Dalton Trans. 41 (2012) 7358–7371 .

[21] I. Bratsos, C. Simonin, E. Zangrando, T. Gianferrara, A. Bergamo, E. Alessio, Dalton Trans. 40 (2011) 9533–9543.

[22] D. Chatterjee, A. Sengupta, A. Mitra, Polyhedron 26 (2007) 178–183.

[23] G.S. Papaefstathiou, A. Sofetis, C.P. Raptopoulou, A. Terzis, G.A. Spyroulias, T.F. Zafiropoulos, J. Mol. Struct. 837 (2007) 5–14.

[24] J.R. Jeitler, M.M. Turnbull, J.L. Wikaira, Inorg. Chim. Acta 351 (2003) 331–344.

[25] N. Gupta, N. Grover, G.A. Neyhart, P. Singh, H.H. Thorp, Inorg. Chem. 32 (1993) 310–316.

[26] K.J. Takeuchi, M.S. Thompson, D.W. Pipes, T.J. Meyer, Inorg. Chem. 23 (1984) 1845–1851.

[27] A. Dovletoglou, S.A. Adeyemi, T.J. Meyer, Inorg. Chem. 35 (1996) 4120–4127.

[28] M.J. Root, E. Deutsch, Inorg. Chem. 24 (1985) 1464–1471.

[29] S.E. Miller, D.A. House, Inorg. Chim. Acta 187 (1991) 125–132.

[30] J.E. Quin, J.R. Devlin, D. Cameron, K.M. Hannan, R.B. Pearson, R.D. Hannan, Biochim. Biophys. Acta, Mol. Basis Dis. 1842 (2014) 802–816.

[31] V. Brabec, Prog. Nucleic Acid Res. Mol. Biol. 71 (2002) 1–68.

[32] C.X. Zhang, S.J. Lippard, Curr. Opin. Chem. Bio. 7 (2003) 481–489.

[33] V. Brabec, O. Novakova, Drug Resist. Updates 9 (2006) 111–122.

[34] J. Liu, W. Zheng, S. Shi, C. Tan, J. Chen, K. Zheng, L. Ji, J. Inorg. Biochem. 102 (2008) 193–202.

[35] T.W. Johann, J. K. Barton, Philos. Trans. R. Soc. London, A 354 (1996) 299–324.

[36] J.G. Vos, J. M. Kelly, Dalton Trans. (2006) 4869–4883.

[37] H. Huang, P. Zhang, Y. Chen, L. Ji, H. Chao, Dalton Trans. 44 (2015) 15602–15610.

[38] A. Tarushi, K. Lafazanis, J. Kljun, I. Turel, A.A. Pantazaki, G. Psomas, D.P. Kessissoglou, J. Inorg. Biochem. 121 (2013) 53–65.

[39] A. Dimitrakopoulou, C. Dendrinou-Samara, A.A. Pantazaki, M. Alexlou, E. Nordlander, D.P. Kessissoglou, J. Inorg. Biochem. 102 (2008) 618–628.

[40] C.V. Kumar, J.K. Barton, N.J. Turro, J. Am. Chem. Soc. 107 (1985), 5518–5523.

[41] A. Tarushi, G. Psomas, C.P. Raptopoulou, D.P. Kessissoglou, J. Inorg. Biochem. 103 (2009) 898–905.

[42] E.S. Koumousi, M. Zampakou, C.P. Raptopoulou, V. Psycharis, C.M. Beavers, S.J. Teat, G. Psomas, T.C. Stamatatos, Inorg. Chem. 51 (2012) 7699–7710.

[43] O. Novakova, H. Chen, O. Vrana, A. Rodger, P.J. Sadler, V. Brabec, Biochemistry 42 (2003) 11544–11554.

[44] D.D. Li, J.L. Tian, W. Gu, X. Liu, S.P. Yan, J. Inorg. Biochem. 104 (2010) 171–179.

[45] M. Jiang, Y. Li, Z. Wu, Z. Liu, C. Yan, J. Inorg. Biochem. 103 (2009) 833–844.

[46] A.R. Timerbaev, C.G. Hartinger, S.S. Aleksenko, B.K. Keppler, Chem. Rev. 106 (2006) 2224–2248.

[47] O. Dömötör, C.G. Hartinger, A.K. Bytzek, T. Kiss, B.K. Keppler, E.A. Enyedy, J. Biol. Inorg. Chem. 18 (2013) 9–17.

[48] Y. Wang, H. Zhang, G. Zhang, W. Tao, S. Tang, J. Lumin. 126 (2007) 211–218.

[49] S. Deepa, A.K. Mishra, J. Pharm. Biomed. Anal. 38 (2005) 556–563.

[50] J.R. Lakowicz, G. Weber, Biochemistry 12 (1973) 4161–4170.

[51] B. Mishra, A. Barik, K.I. Priyadarsini, H. Mohan, J. Chem. Sci. 117 (2005) 641-647.

[52] G. Psomas, D.P. Kessissoglou, Dalton Trans. 42 (2013) 6252–6276.

[53] S. Wu, W. Yuan, H. Wang, Q. Zhang, M. Liu, K. Yu, J. Inorg. Biochem. 102 (2008) 2026–2034.

[54] V. Rajendiran, R. Karthik, M. Palaniandavar, H. Stoeckli-Evans, V.S. Periasamy, M.A. Akbarsha, B.S. Srinag, H. Krishnamurthy, Inorg. Chem. 46 (2007) 8208–8221.

[55] L. Fetzer, B. Boff, M. Ali, X. Meng, J.P. Collin, C. Sirlin, C. Gaiddon, M. Pfeffer, Dalton Trans. 40 (2011) 8869–8878.

[56] B.-J. Han, G.-B. Jiang, J.-H. Yao, W. Li, J. Wang, H.-L. Huang, Y.-J. Liu, Spectrochim. Acta A 135 (2015) 840-849.

[57] M.G. Mendoza-Ferri, C.G. Hartinger, M.A. Mendoza, M. Groessl, A.E. Egger, R.E. Eichinger, J.B. Mangrum, N.P. Farrell, M. Maruszak, P.J. Bednarski, F. Klein, M.A. Jakupec, A.A. Nazarov, K. Severin, B.K. Keppler, J. Med. Chem. 52 (2009) 916-925.

[58] F. Giannini, L.E.H. Paul, J. Furrer, B. Therrienb, G. Suss-Fink, New J. Chem. 37 (2013) 3503-3511.

[59] Y. Mulyana, D.K. Weber, D.P. Buck, C.A. Motti, J.G. Collins, F.R. Keene, Dalton Trans. 40 (2011) 1510-1523.

[60] A.K. Gorle, A.J. Ammit, L. Wallace, F.R. Keene, J.G. Collins, New J. Chem. 38 (2014) 4049-4059.

[61] R.E. Aird, J. Cummings, A.A. Ritchie, M. Muir, R.E. Morris, H. Chen, P.J. Sadler, D.I. Jodrell, Br. J. Cancer 86 (2012) 1652–1657.

[62] Z. Darzynkiewicz, S. Bruno, G. Del Bino, W. Gorczyca, M.A. Hotz, P. Lassota, F. Traganos, Cytometry 13 (1992) 795-808.

[63] D. Wang, S.J. Lippard, Nat. Rev. Drug Discov. 4 (2005) 307–320.

[64] S. Nikolić, L. Rangasamy, N. Gligorijević, S. Aranđelović, S. Radulović, G. Gasser, S. Grgurić-Šipka, J. Inorg. Biochem. In Press, Available online 11 January 2016.

[65] G.M. Almeida, T.L. Duarte, P.B. Farmer, W.P. Steward, G.D. Jones, Int J Cancer 122 (2008) 1810-1819.

Figure/Scheme captions

Fig. 1. Proposed structures of the precursor **P1** and complexes **1** – **3** with the numbering scheme of the Cl-Ph-tpy and bpy ligands used for the NMR characterization.

Fig. 2. The 2D homonuclear ^{1}H-^{1}H COSY NMR spectrum of [Ru(Cl-Ph-tpy)(bpy)Cl]Cl (**3**) in CD_3CN at 298 K.

Scheme 1. Chemical behavior of complexes **1 – 3** in aqueous solution.

Fig. 3. Time-dependence of the absorbance during the aquation of **1** (at 470 nm, 0.05 mM, red squares) and of **2** (at 471 nm, 0.05 mM, blue squares) in H_2O at 298 K. The full lines represent computer fits giving the first order rate constants for the aquation of **1** and of **2**.

Fig. 4. Emission spectra of EB bound to DNA in the presence of complexes **1** (top), **2** (middle) and **3** (bottom). [EB] = 80 μM, [DNA] = 80 μM; [Ru] = 0–80 μM; λ_{ex} = 527 nm. The arrows show the intensity changes upon increased concentrations of the complexes. Insets: plots of I_0/I *versus* [Q]; with (■) are shown the experimental data points and the full line represents the exponential fitting of the data.

Fig. 5. Plot of % relative fluorescence intensity at λ_{em} = 352 nm *vs* r (r = [complex]/[BSA]) for the complexes **1 – 3** (58% of the initial fluorescence intensity for **1**, 68% for **2**, and 81% for **3**) in buffer solution (5 mM Tris and 50 mM NaCl).

Fig. 6. Inverted microscopy examination of HeLa and MRC-5 cells after 72 h of treatment with complex **3**.

Fig. 7. Diagrams representing cell cycle phase distribution of HeLa cells treated with complex **3** or cisplatin (CDDP). IC_{50} values were determined for 72 h agent action. Bar graphs show representative experiments.

Fig. 8. Diagrams representing cell cycle phase distribution of A549 cells treated with complex **3** or cisplatin (CDDP). IC_{50} values were determined for 72 h agent action. Bar graphs show representative experiments.

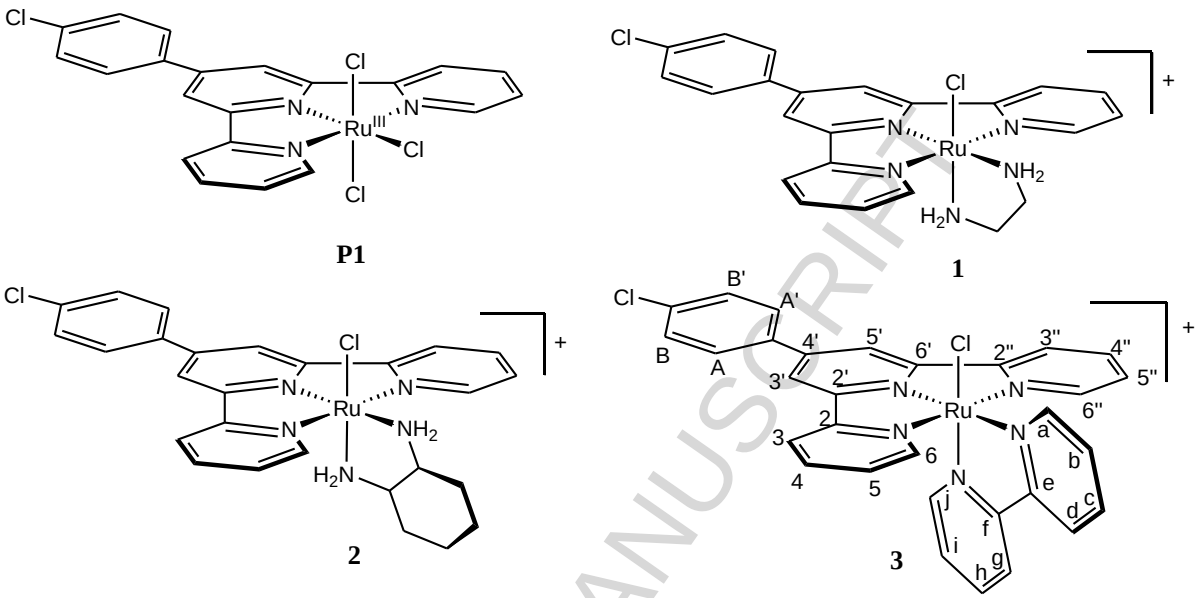

Fig. 1.

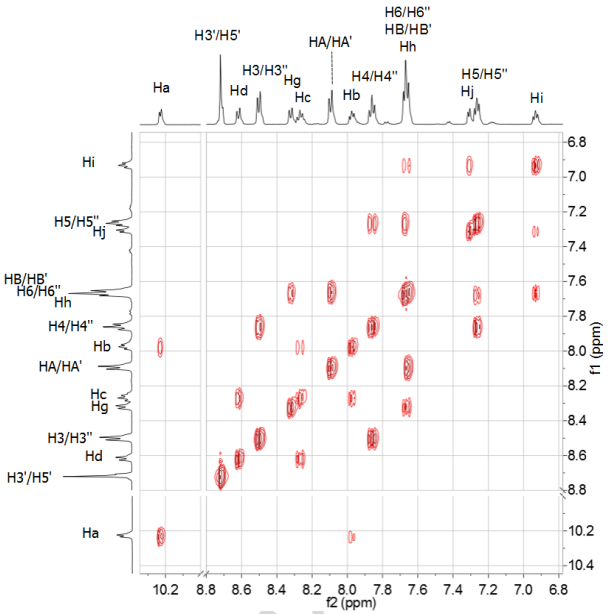

Fig. 2.

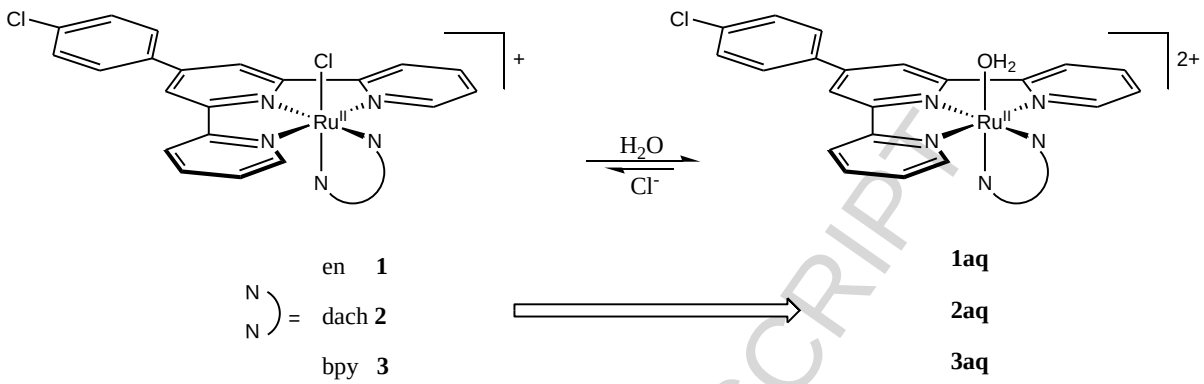

N
N = dach **2**

en **1**

bpy **3**

1aq

2aq

3aq

Scheme 1.

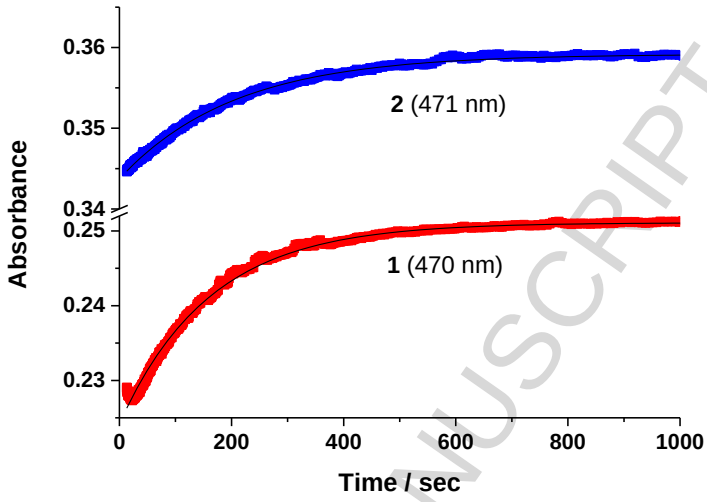

Fig. 3.

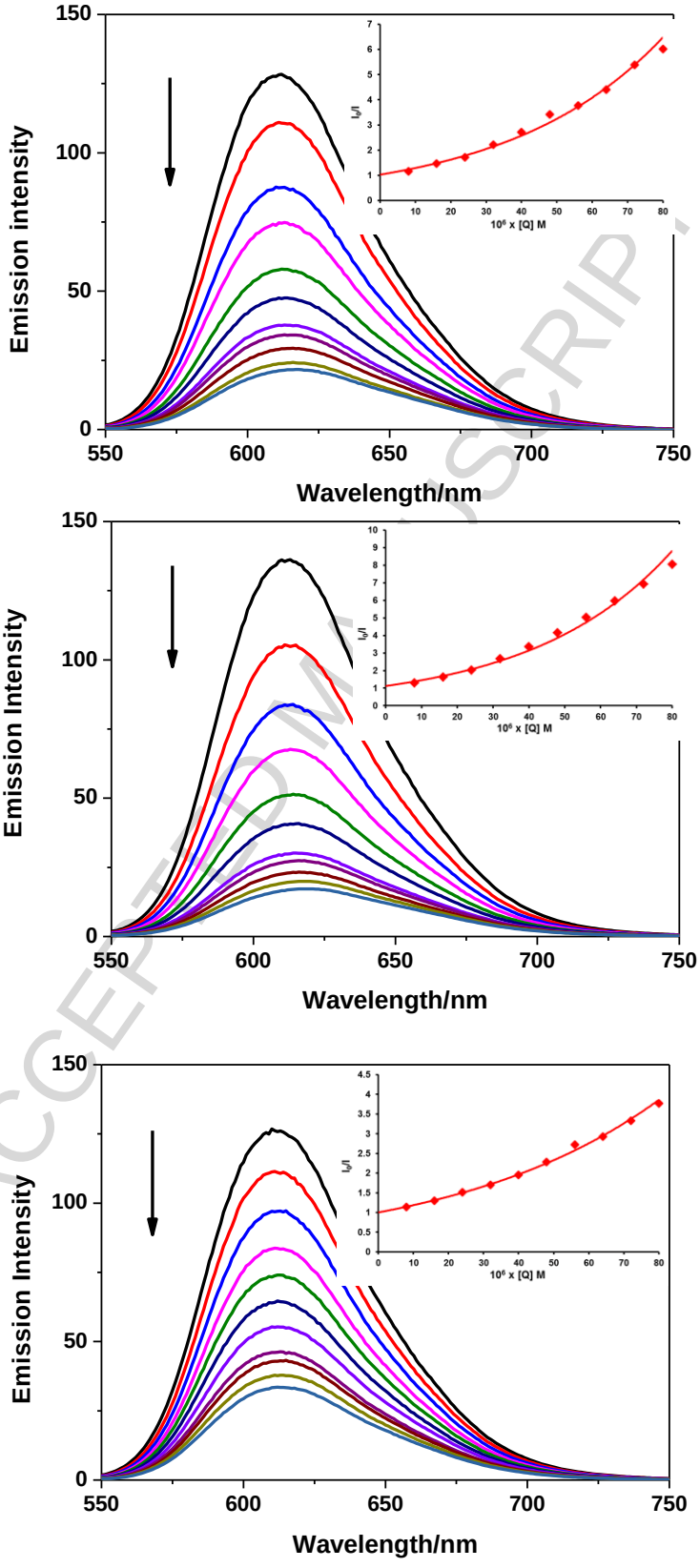

Fig. 4.

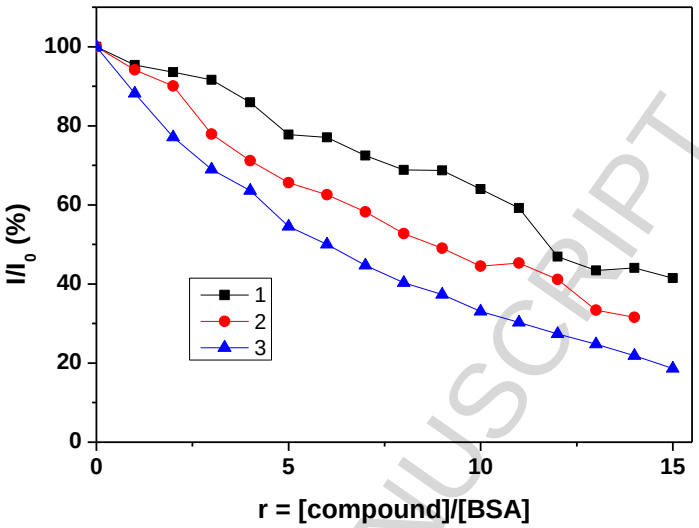

Fig. 5.

HeLa cells

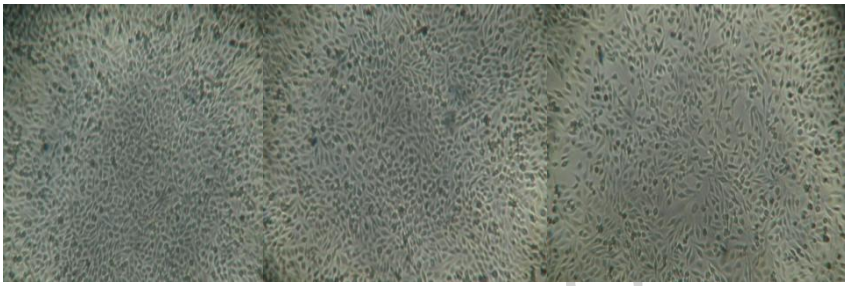

0 μM 6.25 μM 12.5 μM

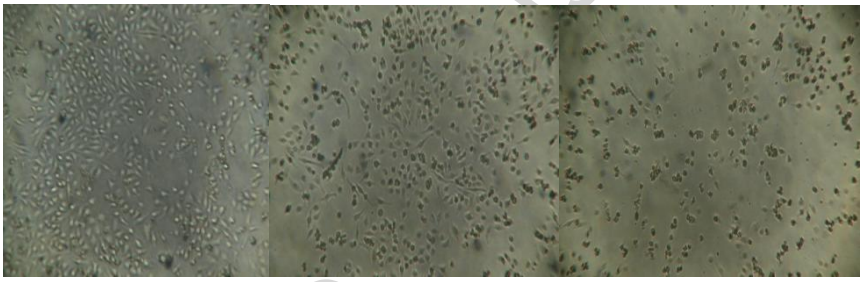

25 μM 50 μM 100 μM

MRC-5 cells

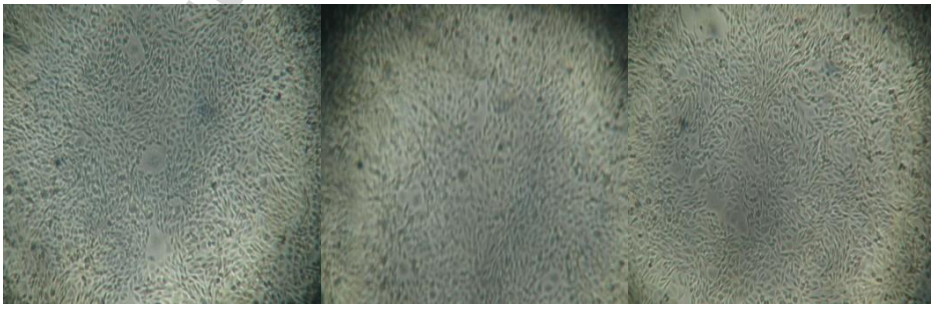

0 μM 6.25 μM 12.5 μM

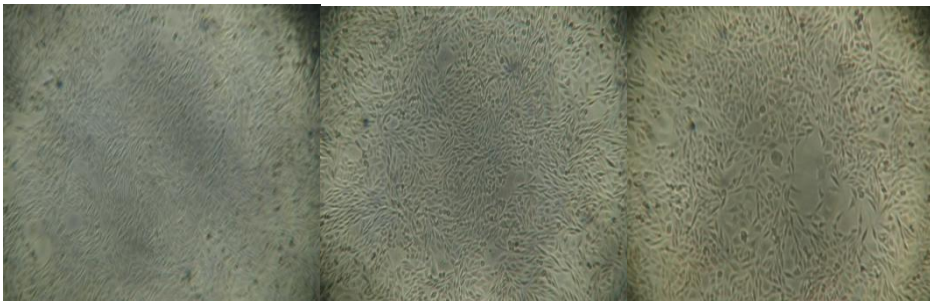

25 μM 50 μM 100 μM

Fig. 6.

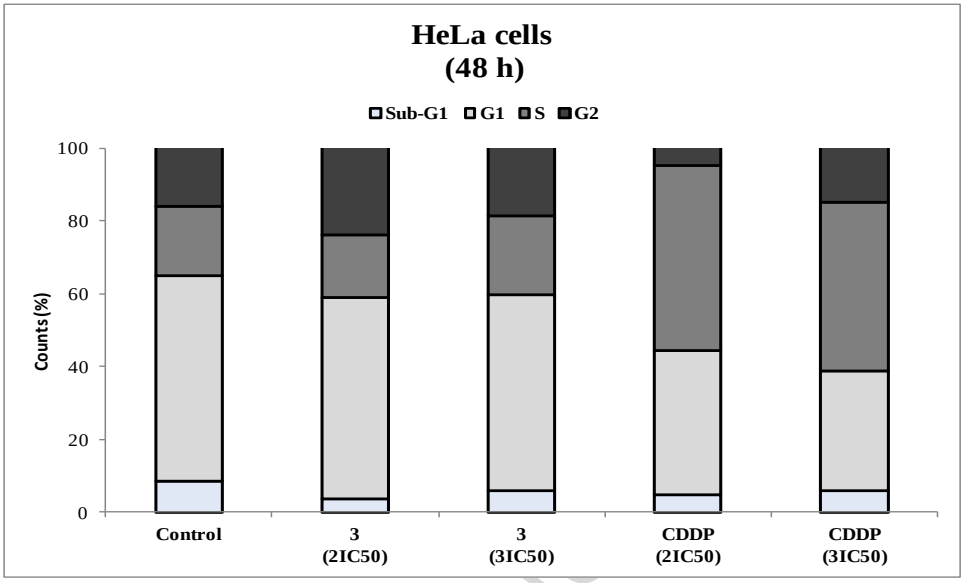

Fig. 7.

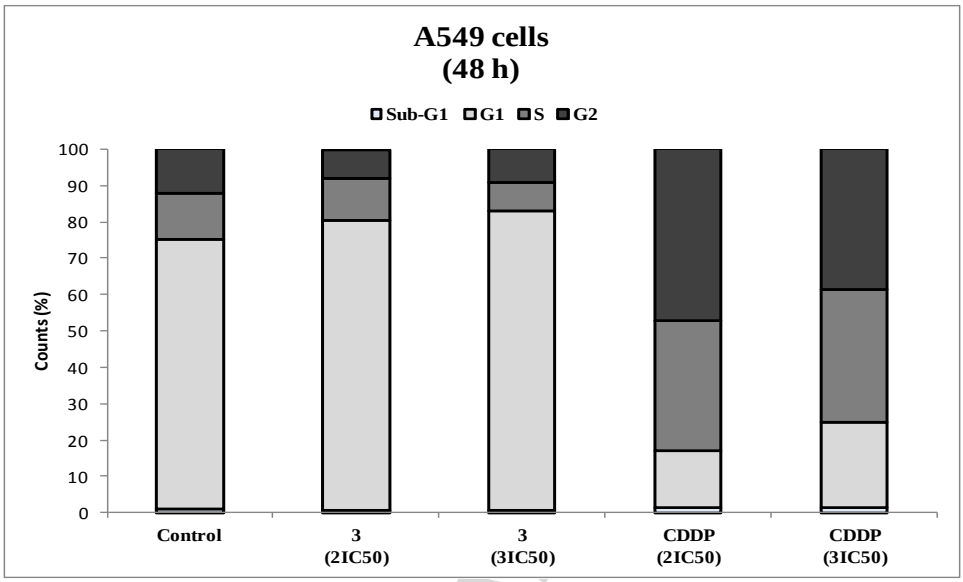

Fig. 8.

Table 1.

Compound	λ_{max} [nm]	λ_{min} [nm]	Isosbestic points [nm]	k_{obs} [$10^{-3}s^{-1}$]	$(t_{1/2})_{H_2O}$ [min]
1	470, 535	394, 579	362, 430, 552	6.10 ± 0.01	2.00 ± 0.03
2	393, 510, 581	471	347, 429, 494	4.90 ± 0.02	2.40 ± 0.02

Table 2.

Complex	K_b [M^{-1}]	K_{sv} [M^{-1}]	V (M^{-1})
1	1.0 (± 0.2) × 10^6	1.9 (± 0.1) × 10^4	1.1 (± 0.3) × 10^4
2	2.8 (± 0.1) × 10^6	2.7 (± 0.1) × 10^4	1.2 (± 0.3) × 10^4
3	9.0 (± 0.2) × 10^6	1.1 (± 0.1) × 10^4	8.9 (± 0.3) × 10^3

Table 3.

Complex	K_{sv} (M^{-1})	k_q ($M^{-1}s^{-1}$)	K (M^{-1})	n	V (M^{-1})
1	3.7 (± 0.4) × 10^4	3.7 (± 0.4) × 10^{12}	2.0 × 10^4	0,81	1.0 (± 0.3) × 10^4
2	4.6 (± 0.5) × 10^4	4.6 (± 0.5) × 10^{12}	3.0 × 10^4	1,50	1.2 (± 0.4) × 10^4
3	3.5 (± 0.07) × 10^4	3.5 (± 0.07) × 10^{12}	5.0 × 10^4	1,34	3.0 (± 0.4) × 10^4

Table 4.

	IC_{50} [μM]		
	HeLa	**A549**	**MRC-5**
1	84.81 ± 4.67	> 100	> 100
2	96.28 ± 3.81	> 100	> 100
3	12.68 ± 1.89	53.80 ± 4.44	97.67 ± 6.93
4	71.23 ± 2.61	> 100	86.66 ± 2.62
5	> 100	> 100	> 100
6	> 100	> 100	> 100
P1	83.05 ± 4.06	> 100	64.87 ± 4.07
Cisplatin	3.33 ± 0.28	5.93 ± 0.66	7.96 ± 0.18

Graphical Abstract

New 4'-(4-chlorophenyl)-2,2':6',2''-terpyridine ruthenium(II) complexes: Synthesis, characterization, interaction with DNA/BSA and cytotoxicity studies

Milan M. Milutinović [a], Ana Rilak [a,*], Ioannis Bratsos [b], Olivera Klisurić [c], Milan Vraneš [d], Nevenka Gligorijević [e], Siniša Radulović [e], Živadin D. Bugarčić [a,*]

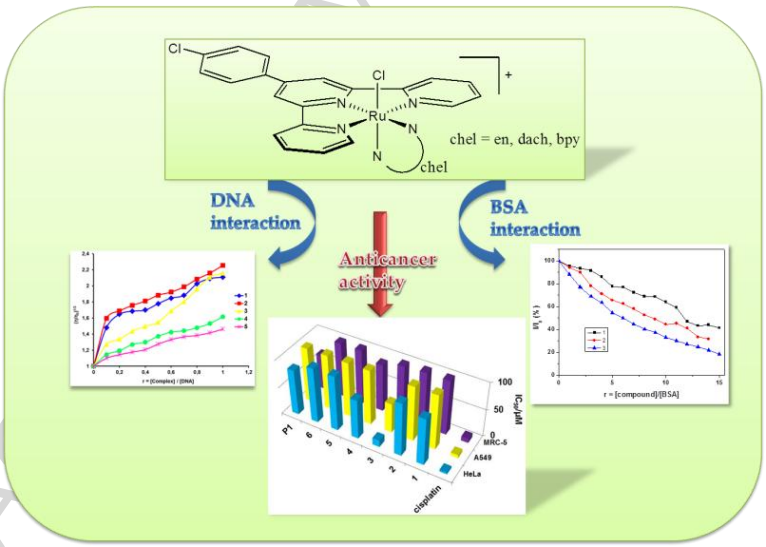

Graphical Synopsis

New 4'-(4-chlorophenyl)-2,2':6',2''-terpyridine ruthenium(II) complexes: Synthesis, characterization, interaction with DNA/BSA and cytotoxicity studies

Milan M. Milutinović [a], Ana Rilak [a,*], Ioannis Bratsos [b], Olivera Klisurić [c], Milan Vraneš [d], Nevenka Gligorijević [e], Siniša Radulović [e], Živadin D. Bugarčić [a,*]

A series of new ruthenium(II)-chlorophenyl-terpyridine complexes were synthesized and fully characterized. The chlorido complexes proved to be labile in aqueous solution and capable of interacting with biomolecules. Furthermore, the complex with bidentate aromatic diamine proved to be superior to those with aliphatic diamines in terms of lipophilicity and biological activity.

Highlights

- Synthesis of new Ru(II) polypyridyl complexes with chlorophenyl-terpyridine ligand.
- All complexes in aqueous solution release the Cl^- ligand to form the aqua species.
- Ruthenium complexes show good binding affinity to DNA and bovine serum albumin.
- The complex with bidentate aromatic diamine displays the highest cytotoxicity.